Aalborg Universitet

AALBORG UNIVERSITY
DENMARK

Fault Diagnosis and System Reconfiguration Strategy of Single-phase Three Level Neutral-Point-Clamped Cascaded Inverter

Pengcheng, Han; He, Xiaoqiong; Ren, Haijun; Wang, Yi; Peng, Xu; Shu, Zeliang; Gao, Shibin; Wang, Yanbo; Chen, Zhe

Fault Diagnosis and System Reconfiguration Strategy of Single-phase Three Level Neutral-Point-Clamped Cascaded Inverter

Pengcheng Han, *Student Member, IEEE*, Xiaoqiong He* *Member, IEEE*, Haijun Ren, Yi Wang, Xu Peng, Zeliang Shu, *Senior Member, IEEE*, Shibin Gao, Yanbo Wang *Member, IEEE*, Zhe Chen, *fellow, IEEE*

Abstract— **This paper presents a fault diagnosis method and system reconfiguration strategy of three level neutral-point-clamped cascaded inverter (3L-NPC-CI) to enhance reliability of power supply in electrified railway. First, neural network is employed to perform open-circuit fault diagnosis and identify fault switches. Then, system reconfiguration strategy is proposed to perform single phase 3L-NPC-CI reconfiguration. Through the analysis of the operation status of 3L-NPC, there are eight fault modes in single bridge arm, including single-switch fault and double-switches fault. By the feature analysis for the output arm voltage harmonic of normal and eight fault modes, seven harmonic parameters are selected as fault feature vectors. Meanwhile, a three-layer neural network is constructed, and the seven feature vectors are the input layer of the neural network. By training algorithm, the fault switches location can be identified accurately about one modulation period. Then, the fault module is bypassed and the 3L-NPC-CI system is stable by reconfiguring the modulation strategy of other normal modular. Simulation and experimental results are given to validate the proposed fault diagnosis and system reconfiguration strategy. The proposed method is able to improve robustness and reliability of 3L-NPC-CI in traction power supply system.**

Index Terms— **Fault diagnosis, Neural network, Modulation re configuration, Single-phase 3L-NPC-CI, Spectrum analysis.**

I. INTRODUCTION

Advanced co-phase traction power supply system (ACTPSS) is the development trend of the traction power supply system in the future [1]-[2]. ACTPSS is an attractive and promising solution to achieve superior power quality in traction power supply system, which is shown in Fig.1. Single-phase three level neutral-point-clamped cascaded inverter (3L-NPC-CI) is the most commonly used topology for ACTPSS, due to the 3L-NPC-CI has a better performance applied to high voltage and high power applications [3]-[6]. More than hundreds of IGBTs are used in single-phase 3L-NPC-CI, while power device is the most fragile component. The faults statistics analysis from [7]-[8] show that power devices take commonly high fault proportion in power converter. The presence of faults will undoubtedly degrade the safety and reliability of traction power system. Reliability is one of important concerns in traction power supply system. Hence, the efforts toward reliability enhancement in traction power supply system should be performed. Fault diagnosis and reconfiguration strategy of 3L-NPC-CI are important aspects for reliability enhancement.
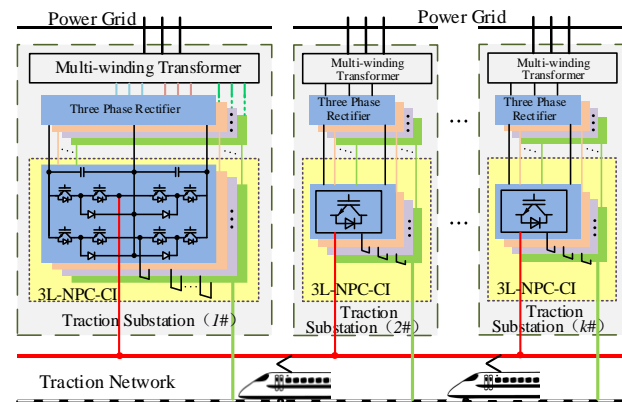

Fig.1 System configuration of ACTPSS

Open-circuit fault (OCF) is the main fault type for power electronic component. The fault diagnosis of H-bridge converter has been researched for a long time [12-15]. Compared with the H-bridge converter, the 3L-NPC converter has more switch states. In this way, the open fault detection of 3L-NPC converter is more complex, especially in cascaded system.

OCFs diagnosis methods including current-based methods and voltage-based methods have been paid much attentions [10]-[26]. In [16]-[18], current-based fault diagnosis methods are developed to identify fault characteristics during a switching period, where corresponding diagnosis thresholds are set to perform fault diagnosis. However, the current-based methods are not effective for time-variant loads in traction power supply system. The load changes dramatically especially no-load situation since the current cannot be detected [19].

Another powerful strategy is voltage-based fault diagnosis methods [20]-[22], where measured voltage and reference command are compared to identify the difference and locate

(birdhpc@163.com, haidaoren@outlook.com, de_yiwang@163.com, shuzeliang@swjtu.edu.cn, gao_shi_bin@126.com)
Civil Aviation Flight University of China, Guanghan, China. CO 618307, (pengxuswjtu@foxmail.com)
Aalborg University, Department of Energy Technology. CO 9220, Denmark (ywa@et.aau.dk, zch@et.aau.dk)

faults. However, voltage-based method is not applicable for OCFs since voltage measurements are almost not affected. [21] proposed a method by using the inherent PWM characteristic of the output voltage, but the location of a fault switch could not be identified. [22] can realize the location of single-switch fault. However, it is difficult to realize the precise diagnosis in lots of complex fault modes, especially in a cascaded inverter.

For cascaded converters, there are more switching devices and fault modes. In order to implement accurate diagnosis for different fault modes, more fault features should be identified. There are different harmonic components contained in the output voltage. The fault characteristics can be obtained by the arm bridge voltage under different fault modes, which can be used to achieve fault diagnosis. Therefore, the harmonic detection method is used in this paper. In order to make full use of fault characteristics, neural network (NN) based fault diagnosis is the most commonly used method [23-26]. The possibilities offered by neural network for fault diagnosis and system identification are investigated in [25]. And the literature [26] presents artificial NN for real-time fault detection of power switches. NN techniques do not require any mathematical models, and it could learn from big data to classify faults. Above of these methods, neural network can be applied in fault classification of single-phase 3L-NPC-CI.

Once faults are identified, system reconfiguration and fault-tolerant methods can be implemented to enhance safety and reliability of system. The literature [27] utilizes an active NPC topology for the fault-tolerant operation, instead of NPC topology. In [28]-[30], auxiliary components and redundant circuits are added in power converter to implement system reconfiguration. However, the application of active NPC topology and redundant circuit increase hardware cost of power converter. In [31], the fault diagnosis method based on NN and system reconfiguration strategy is proposed, but only the single-switch fault is proved in the simulation and the experiment.

Therefore, this paper presents a neural network-based fault diagnosis method and system reconfiguration strategy for 3L-NPC-CI system. Neural network is a nonlinear model with multiple inputs and outputs, which is able to approximate input-output relationship of dynamic system instead of using mathematical model. Compared with the voltage-based and current-based methods, NN-based method can realize the fault diagnosis of more kinds of OCFs and diagnose OCFs fast and accurately. As a result, NN-based method is more suitable for cascaded converter, which has plenty of fault modes.

The rest of this paper is organized as follows. In Section II, the topology, the modulation strategy and control method of 3L-NPC-CI are introduced. Fault mechanism and characteristics are explained in Section III, where the feature vectors are set up according to fault mechanism analysis. In Section IV, neural network-based fault diagnosis method for 3L-NPC-CI is proposed. And a reconfiguration strategy under OCFs is presented in Section V. On the basis of theoretical analysis, simulation and experimental results are given to validate the proposed fault diagnosis method and reconfiguration strategy in Section VI. Conclusion is summarized in Section VII.

II. SYSTEM CONFIGURATION

A. Structure of Single-Phase 3L-NPC-CI

Fig. 2 shows topological structure of single-phase 3L-NPC-CI, where Module i consists of Arm a and Arm b.
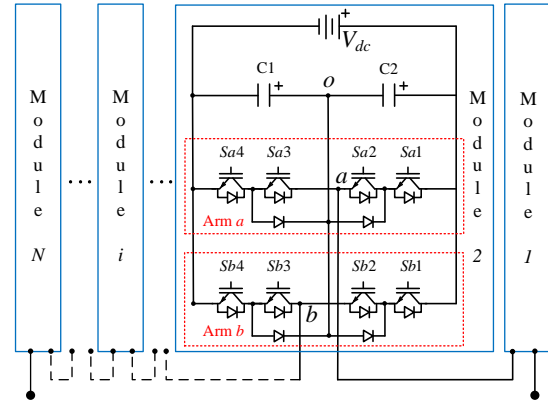

Fig.2 Topological structure of single-phase 3L-NPC-CI

Normally, three different voltage levels ($+V_{dc}$, 0, $-V_{dc}$) can be obtained with an individual arm. A five-level output voltage can be achieved by composed two arms of NPC. For example, as for one module, relations between output voltage level and switch status are shown in Table I.

TABLE I VOLTAGE LEVEL AND SWITCH MODE

Level	S_{a1}	S_{a2}	S_{a3}	S_{a4}	S_{b1}	S_{b2}	S_{b3}	S_{b4}
V_{dc}	1	1	0	0	0	0	1	1
$0.5V_{dc}$	1	1	0	0	0	1	1	0
	0	1	1	0	0	0	1	1
	1	1	0	0	1	1	0	0
0	0	0	1	1	0	0	1	1
	0	1	1	0	0	1	1	0
$-0.5V_{dc}$	0	0	1	1	0	1	1	0
	0	1	1	0	1	1	0	0
$-V_{dc}$	0	0	1	1	1	1	0	0

B. Modulation Strategy of Single Phase 3L-NPC-CI

In this paper, Phase opposition disposition SPWM (POD-SPWM) strategy is used in the single module and Carrier phase shifted SPWM (CPS-SPWM) strategy is used in the cascaded module.

Fig.3 shows modulation strategy of single-phase 3L-NPC-CI module. POD-SPWM strategy is applied for each individual arm. In Fig.3, C_{a1} and C_{a2} are triangular carriers of Arm a, u_a represents modulation wave of Arm a. The phase of C_{a1} is opposite with C_{a2}. When the value of u_a is higher than C_{a1}, S_{a1} and S_{a2} are switched on. When the value of u_a is lower than C_{a2}, S_{a3} and S_{a4} are switched on. In the other case, S_{a2} and S_{a3} are turned on, and the output level is 0. Similarly, C_{b1} and C_{b2} are triangular carriers of arm b, u_b represents modulation wave of arm b. The phase difference between C_{a1} and C_{b1} is π.
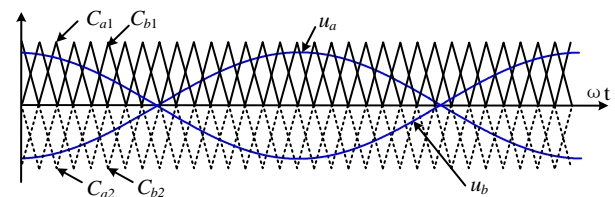

Fig.3 Modulation strategy of single phase 3L-NPC-CI

CPS-SPWM strategy is adopted for single-phase 3L-NPC-CI

because of the good performance for the cascaded system. Modulation strategy of every single module is the same. It is noted that whenever N (number of cascaded NPC modules) is odd or even number, the triangular carriers of these modules sequentially move forward π/N. Besides, M represents modulation index in this paper.
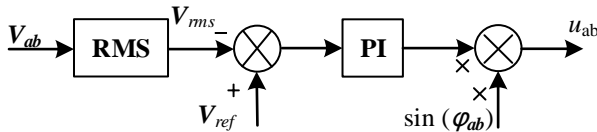
C. Voltage Closed-loop Control Strategy

Fig.4 Voltage closed-loop control of single phase 3L-NPC-CI

Fig.4 is the voltage closed-loop control of single phase 3L-NPC-CI. V_{ab} is the output voltage which is sampled by the controller. V_{rms} is the effective value of V_{ab}. V_{ref} is the reference value of V_{rms}. The error of V_{rms} and V_{ref} is input to PI controller. The modulation signal u_{ab} is the value obtained by multiplying $\sin(\varphi_{ab})$ and the result of the PI controller.

III. FAULT MECHANISM AND FEATURES ANALYSIS
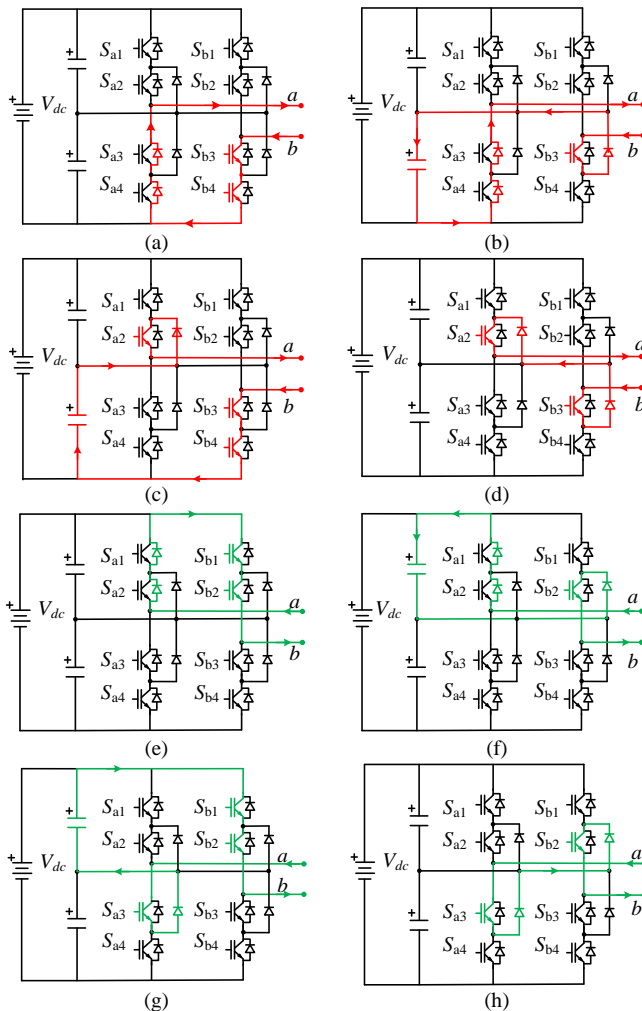

(a)　(b)

(c)　(d)

(e)　(f)

(g)　(h)

Fig.5 Fault current paths (OCFs of Arm a).

In this section, Fault mechanism and characteristics are explained, where the feature vectors are set up according to fault mechanism analysis.

A. Fault switch modes

When OCFs occur in a bridge of single-phase 3L-NPC module, there are eight specific fault modes of Arm a. Considering CPS+POD PWM strategy, there are eight fault current paths, which are shown in Fig.5. It is defined that currents directions in Fig.5 (a)-(d) are positive, and those in Fig.5 (e)-(h) are negative. Relationships between fault switch modes and fault current paths are shown in TABLE II.

TABLE II
FAULT SWITCH SIGNAL AND FAULT CURRENT CURRENT PATHS

Fault current path		Fault switch signals S_{a1}-S_{a4}	Switch signals S_{b1}-S_{b4}
Positive current	a	1000 / 0010 / 0000	0011
	b	1000 / 0010 / 0000	0110
	c	0100	0011
	d	0100	0110
Negative current	e	0001 / 0100 / 0000	1100
	f	0001 / 0100 / 0000	0110
	g	0010	1100
	h	0010	0110

B. Fault modes and mechanism

Output voltage of the arm would be abnormal in the presence of OCFs. With different types of faults, output voltages of the arm are also different under different types of faults. Take an example of bridge Arm a to describe the analysis of fault mechanism. OCFs can be divided into two types, which are only in the upper/lower half of one bridge arm or both in the upper and lower half of one bridge arm. The V_{ao} is shown in Fig.6 when NPC is in normal condition, where V_{ao} is the output voltage of Arm a.
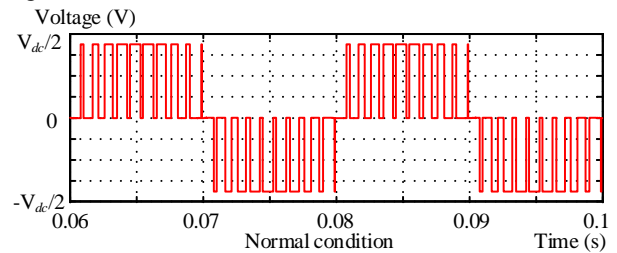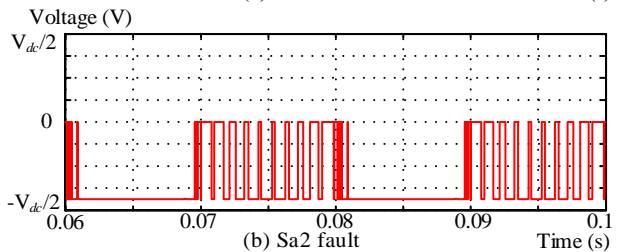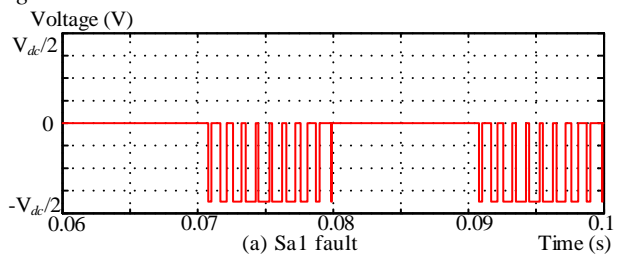

Fig.6 Normal output waveform of arm a.

1) Fault switches are only in the upper/lower half of one bridge arm

(a) Sa1 fault

(b) Sa2 fault

This article has been accepted for publication in a future issue of this journal, but has not been fully edited. Content may change prior to final publication. Citation information: DOI 10.1109/TIA.2019.2901359, IEEE Transactions on Industry Applications

> REPLACE THIS LINE WITH YOUR PAPER IDENTIFICATION NUMBER (DOUBLE-CLICK HERE TO EDIT) <   4
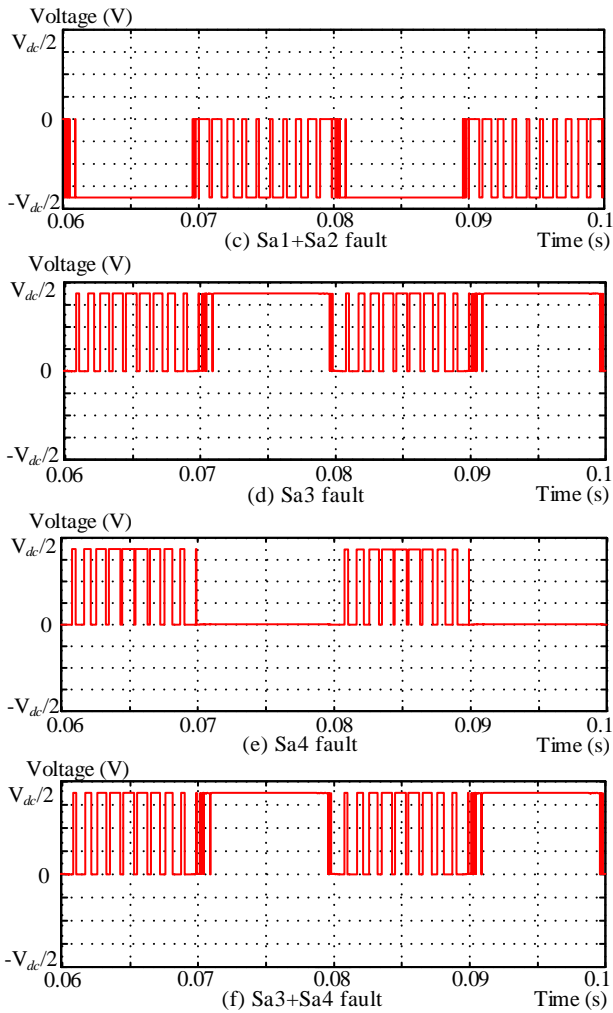
Fig.7 Output voltage of V_{ao} when fault in the same half of one bridge arm.

There are six fault modes in this type. V_{ao} is shown in Fig.7 with different fault tapes. As can be seen in Fig.7, V_{ao} in S_{a2} fault is exactly the same as the V_{ao} in $S_{a1}+S_{a2}$ fault, and V_{ao} in S_{a3} fault is the same as the V_{ao} in $S_{a3}+S_{a4}$ fault. Therefore, the same steps will be replaced when a failure occurs at S_{a2} or $S_{a1}+S_{a2}$ and S_{a3} or $S_{a3}+S_{a4}$. Based on that, faults classification could be simplified as S_{a1} fault, S_{a2} fault, S_{a3} fault and S_{a4} fault.

a)   Fault mode 1, S_{a1} fault

As shown in TABLE III, when current is positive, switch signal 1100 cannot be obtained, and it is converted to 0100. The current paths are shown in Fig.5 (c)-(d), so that the output voltage level is 0. When current is negative, switch signals are not changed, so that output voltage of V_{ao} is the same as normal conditions.

TABLE III
SWITCH SIGNALS CONVERSION OF ARM a (S_{a1} FAULT)

Normal switch signal Sa1-Sa4	Switch signal of Sa1 fault Sa1-Sa4
1100	0100
0110	0110
0011	0011

b)   Fault mode 2, S_{a2} fault

As shown in TABLE IV, when current is positive, switch signal 1100 is conversed to 1000, and switch signal 0110 is converted to 0010. The current paths are shown in Fig.5 (a)-(b),

so that the output voltage level is $-V_{dc}/2$. When current is negative, switch signal 0110 is converted to 0010, which can get the zero level, so that output voltage of V_{ao} is the same as normal conditions. The current paths are shown in Fig.5 (g)-(h).

TABLE IV
SWITCH SIGNALS CONVERSION OF ARM a (S_{a2} FAULT)

Normal switch signal Sa1-Sa4	Switch signal of Sa2 fault Sa1-Sa4
1100	1000
0110	0010
0011	0011

c)   Fault mode3, S_{a3} fault/$S_{a3}+S_{a4}$ fault

As shown in TABLE V, when current is positive, switch signal 0110 is converted to 0100, which can output the zero level, so that output voltage of V_{ao} is the same as normal conditions. The current paths are shown in Fig.5 (c)-(d). When current is negative, switch signal 0110 and 0011 are converted to 0100 and 0001. The current paths are shown in Fig.5 (e)-(f). In this way, the output voltage level is $V_{dc}/2$.

TABLE V
SWITCH SIGNALS CONVERSION OF ARM a (S_{a3} FAULT)

Normal switch signal Sa1-Sa4	Switch signal of Sa3 fault Sa1-Sa4
1100	1100
0110	0100
0011	0001

d)   Fault mode4, S_{a4} fault

As shown in TABLE VI, when current is positive, the output voltage of V_{ao} remains the same. When current is negative, switch signal 0011 cannot be obtained, and it is conversed to 0010, so that output voltage level is 0. The current paths are shown in Fig.5 (g)-(h).

TABLE VI
SWITCH SIGNALS CONVERSION OF ARM a (S_{a4} FAULT)

Normal switch signal Sa1-Sa4	Switch signal of Sa4 fault Sa1-Sa4
1100	1100
0110	0110
0011	0010

2) Fault switches are both in the upper and lower half of one bridge arm
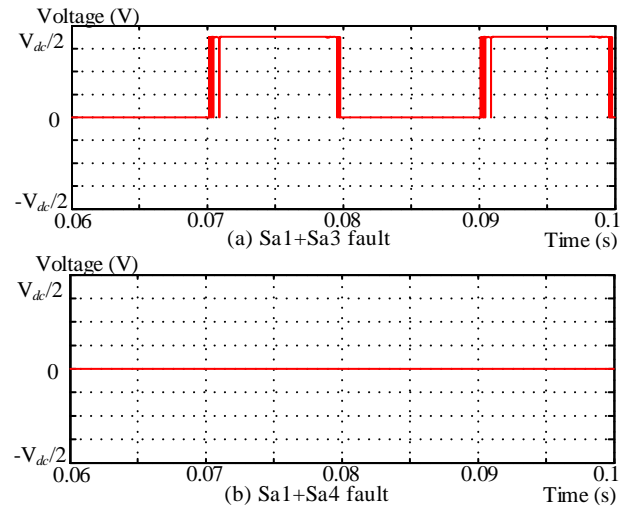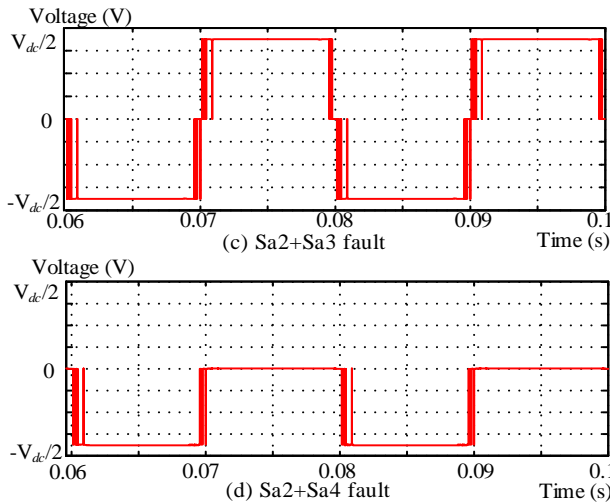
Fig.8 Output voltage of V_{ao} when fault in both half of one bridge arm.

There are four fault modes in this type, which are $S_{a1}+S_{a3}$ fault, $S_{a1}+S_{a4}$ fault, $S_{a2}+S_{a3}$ fault and $S_{a2}+S_{a4}$ fault. The output voltage of V_{ao} is shown in Fig.8.

a)   Fault mode5, $S_{a1}+S_{a3}$ fault

As shown in TABLE VII, when current is positive, switch signal 1100 and 0110 are both conversed to 0100, so that output voltage level of V_{ao} is 0. The current paths are shown in Fig.5 (c)-(d). When current is negative, switch signal 0110 and 0011 are both conversed to 0001. As a result, output voltage level of V_{ao} is $V_{dc}/2$. The current paths are shown in Fig.5 (e)-(f).

TABLE VII
SWITCH MODES CONVERSION OF ARM a ($S_{a1}+S_{a3}$ FAULT)

Normal switch signal Sa1-Sa4	Switch signal of Sa1+ Sa3 fault Sa1-Sa4
1100	0100
0110	0100
0011	0001

b)   Fault mode6, $S_{a1}+S_{a4}$ fault

As shown in TABLE VIII, when current is positive, switch signal 1100 is converted to 0100. When current is negative, switch signal 0011 is converted to 0010. The current paths are shown in Fig.5 (a)-(b) and Fig (e)-(f). Therefore, the output voltage level of V_{ao} is 0 when current is positive and negative.

TABLE VIII
SWITCH MODES CONVERSION OF ARM a ($S_{a1}+S_{a4}$ FAULT)

Normal switch signal Sa1-Sa4	Switch signal of Sa1+ Sa4 fault Sa1-Sa4
1100	0100
0110	0110
0011	0010

c)   Fault mode7, $S_{a2}+S_{a3}$ fault

As shown in TABLE IX, switch signal 1100, 0110, and 0011 are converted to 1000, 0000 and 0001. Whenever current is positive and negative, the output voltage level of V_{ao} is $-V_{dc}/2$ and $V_{dc}/2$. The current paths are shown in Fig.5 (c)-(d) and Fig (g)-(h).

TABLE IX
SWITCH MODES CONVERSION OF ARM a ($S_{a2}+S_{a3}$ FAULT)

Normal switch signal Sa1-Sa4	Switch signal of Sa2+ Sa3 fault Sa1-Sa4
1100	1000
0110	0000
0011	0001

d)   Fault mode8, $S_{a2}+S_{a4}$ fault

As shown in TABLE X, when current is positive, switch signal 1100 and 0110 are converted to 1000 and 0010, so that the output voltage level is $-V_{dc}/2$. When current is negative, switch mode 0110 and 0011 are both converted to 0010. In this way, the output voltage level is 0. The current paths are shown in Fig.5 (a)-(b) and Fig (g)-(h).

TABLE X
SWITCH MODES CONVERSION OF ARM a ($S_{a2}+S_{a4}$ FAULT)

Normal switch signal Sa1-Sa4	Switch signal of Sa2+ Sa4 fault Sa1-Sa4
1100	1000
0110	0010
0011	0010

C. Fault features

According to fault mechanism analyses, the V_{ao} of fault S_{a1} and S_{a4} are symmetric, but the phases of V_{ao} are different in these two faults. The phases of V_{ao} in S_{a1} fault is delayed by T/2 from the phases of V_{ao} in S_{a4} fault, where T is the modulation period time.

It can be expressed as $U_1(t)=-U_2(t+T/2)$. Theoretically, *i*-th harmonic amplitudes, odd harmonic phase and THD of S_{a1} fault are the same as S_{a4} fault, but the phase difference of even harmonic is π. S_{a2} fault and S_{a3} fault have the same symmetry. Moreover, $S_{a1}+S_{a3}$ fault and $S_{a2}+S_{a4}$ fault have exactly the same symmetry as well. Because fault waveforms are periodic, output spectrum of one bridge leg could be expressed with FFT, which is as follows.

$$F_a(\omega_c t, \omega_v t) = \frac{M}{2}\cos(\omega_v t) \pm \frac{2}{m\pi} e^{-jm\alpha} \sum_{m=1,2,\cdots}^{\infty} \sum_{n=\pm1,\pm3,\cdots}^{\pm\infty}$$
$$[J_n(\frac{mM\pi}{2}) \cdot \sin(m\omega_c t + n\omega_v t + n\frac{\pi}{2})] \quad (1)$$

Where
J_n Bessel function.
M modulation index.
ω_v angular velocity of modulation wave.
ω_c angular velocity of triangular carrier.

In (1), *m* represents *m* times carrier frequency, *n* （$n = \pm1$, $\pm3\ldots$） represents odd harmonics. The FFT results of V_{ao} in normal and eight fault modes are shown in Fig.9. The Fig.9 (a) is the normal output voltage spectrum. The output spectrum does not contain carrier harmonic component and low order harmonics. The Fig.9 (b)-(e) are the output voltage spectrums when the single-switch faults occur. Comparing these four pictures with normal mode, the DC voltage, low order harmonics, and carrier harmonic component are contained. The fundamental wave amplitude is reduced. Moreover, the 2-nd harmonic amplitude and 3-rd harmonic amplitude are different between S_{a1} fault (S_{a4} fault) and S_{a2} fault (S_{a3} fault). Then, the S_{a1} fault (S_{a2} fault) and S_{a4} fault (S_{a3} fault) can be determined by detecting the phase of fundamental wave and 2-nd harmonic phase. Similarly, the characteristics of double-tube faults are the same. Specially, the harmonic amplitude of $S_{a2}+S_{a3}$ fault is zero because there is no output voltage in this status. According to the analysis above all, values of DC amplitude, fundamental wave amplitude, 2-nd harmonic amplitude, 3-rd harmonic

amplitude, carrier frequency harmonic amplitude and fundamental wave phase, 2-nd harmonic phase are selected as the feature vectors.
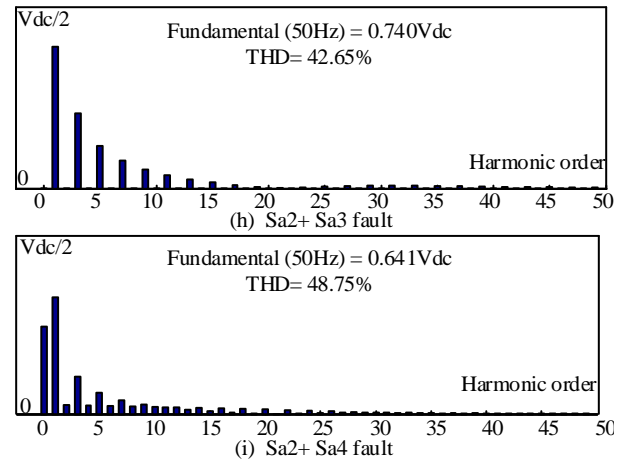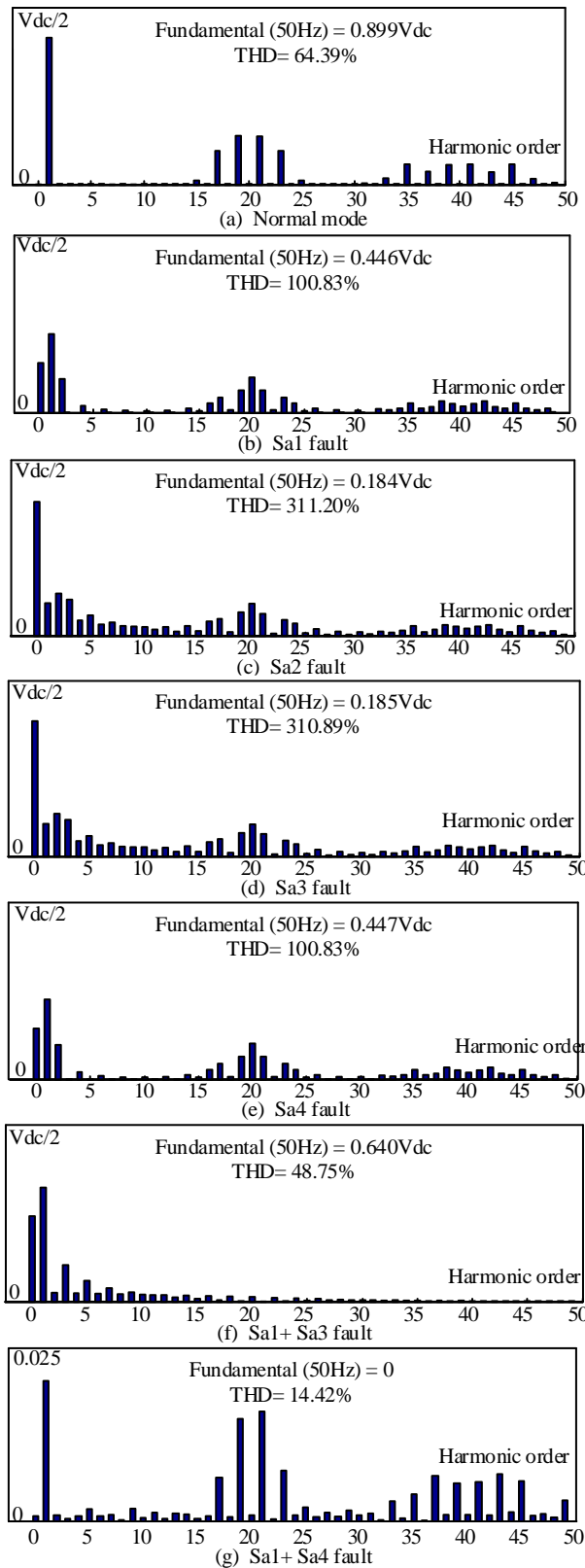

(a) Normal mode

(b) Sa1 fault

(c) Sa2 fault

(d) Sa3 fault

(e) Sa4 fault

(f) Sa1+ Sa3 fault

(g) Sa1+ Sa4 fault

(h) Sa2+ Sa3 fault

(i) Sa2+ Sa4 fault

Fig. 9 Output voltage spectrum of Arm a

IV. THE PROPOSED NN-BASED FAULT DIAGNOSIS

In this section, NN-based fault diagnosis for single-phase 3L-NPC-CI is proposed. Neural network is a nonlinear model with multiple inputs and outputs, which is able to approximate input-output relationship of dynamic system instead of using mathematical model. Since the control system is hardly to recognize different fault types, it is necessary to find a method which can diagnose different types of faults precisely. Normal mode and eight fault modes are numbered by fault output vectors as shown in TABLE XI.

TABLE XI
FAULT MODES AND OUTPUT OF NEURAL NETWORK

Mode	Output vector
Normal mode	1 0000 0000
Fault mode 1	0 1000 0000
Fault mode 2	0 0100 0000
Fault mode 3	0 0010 0000
Fault mode 4	0 0001 0000
Fault mode 5	0 0000 1000
Fault mode 6	0 0000 0100
Fault mode 7	0 0000 0010
Fault mode 8	0 0000 0001
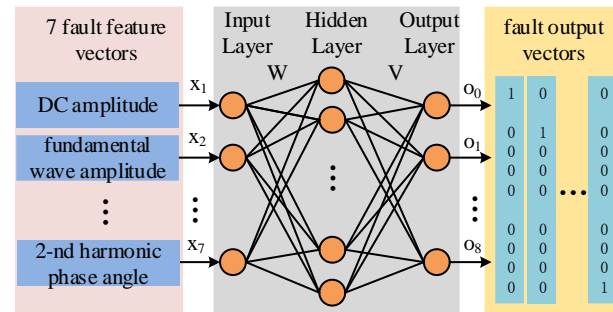
Fig.10. Diagram of Neural network

In this work, a three-layer neural network is employed to identify OCF modes of single-phase 3L-NPC-CI, which consists of input layer, hidden layer and output layer. Fig. 10 shows the diagram of neural network. x_1, x_2, … x_n are input signals. The x_i is the input signals of 7 fault feature vectors, including DC amplitude, fundamental wave amplitude, 2-nd harmonic amplitude, 3-rd harmonic amplitude, switching-

This article has been accepted for publication in a future issue of this journal, but has not been fully edited. Content may change prior to final publication. Citation information: DOI 10.1109/TIA.2019.2901359, IEEE Transactions on Industry Applications

> REPLACE THIS LINE WITH YOUR PAPER IDENTIFICATION NUMBER (DOUBLE-CLICK HERE TO EDIT) <   7

frequency harmonic amplitude, fundamental wave phase angle and 2-nd harmonic phase angle. u_i represents the internal status. $w_{1i}, w_{2i}, \ldots w_{ni}$ are weight coefficients between (1-st…n-th) the neuron of the input layer and i-th neuron in the output layer. The o_i is the output vector of the normal mode and 8 fault modes, which are defined in TABLE XI. The output equation is then given as (2),

$$u_i = \sum_{j=1}^{n} w_{ji} x_j + \theta_i = W_i^T X \qquad (2)$$

Where $W_i = [w_{1i}, w_{2i}, \cdots, w_{ni}]^T$, $X = [x_1, x_2, \cdots, x_n]^T$

θ_i is threshold value.

The threshold function applied in this work is defined as (3) and (4).

$$y_i = f(u_i) \qquad (3)$$

$$y_i = \frac{2}{1+\exp(-2u_i)} - 1 = \frac{2}{1+\exp(-2\sum_{j=1}^{n} w_{ji} x_j - 2\theta_i)} - 1 \qquad (4)$$

Input layer consists of 7 neurons, which is corresponding to a 7-dimensional fault feature input vector $[x_1, x_2, \ldots x_7]^T$. The output layer consists of 9 neurons, which can output a 9-dimensional vector $[o_0, o_2, \ldots o_8]^T$. The output vector represents the normal mode or 8 fault modes. In Fig.10, w is weight matrix between the input layer and the hidden layer, and V is weight matrix between the hidden layer and the output layer, $w = [w_1, w_2, \ldots w_8]$, $v = [v_1, v_2, \ldots v_9]$.

Effective function of output layer is linear function,

$$o_m = \sum_{i=1}^{8} v_{im} y_i + \lambda_m \qquad (5)$$

Where λ_m is the threshold value. Values of fault feature vectors ($M = 0.6, 0.65, 0.7, 0.75, 0.8, 0.85, 0.9, 0.95$) are counted as training samples. Gradient descent method is adapted for training NN. Error function is defined as,

$$E_p = \frac{1}{2} \sum_{m=1}^{9} (t_m - o_m)^2 \qquad (6)$$

t_m is theoretical expectation. Adjustment amount of weight value each time,

$$\Delta V_{im} = -\eta \frac{\partial E_p}{\partial V_{im}} \qquad (7)$$

η is learning rate($0 < \eta < 1$). Adjustment amount of weight value between output layer and hidden layer is,

$$\Delta v_{im} = \eta \delta_m y_i \qquad (8)$$

In (8), $\delta_m = o_m(1 - o_m)(t_m - o_m)$.

Adjustment amount of weight value between the input layer and hidden layer is,

$$\Delta w_{ni} = \eta \delta_i x_n \qquad (9)$$

In (9), $\delta_i = y_i(1 - y_i)\Sigma\delta_m v_{im}$.

The NN parameters for training is set up in this paper. Based on training samples, results are obtained via NN forward-propagation. If the desired value is not achieved, the error signal will be propagated backward and adjusted parameters of NN. The convergence curve of NN is shown in Fig.11, After 264 pieces of training, the mean square error of NN meet the minimum mean square error requirements. NN is tested by testing samples, and the NN can realize fault diagnosis after the well trained.
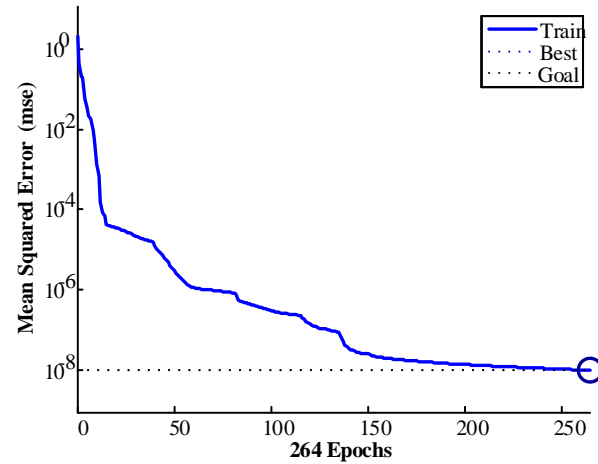

Fig.11 Convergence curve of neural network

V. RECONFIGURATION STRATEGY

Once the faults are identified, reconfiguration strategy can be developed to implement fault-tolerant control. Fig. 12 shows diagram of the proposed fault diagnosis and reconfiguration strategy.
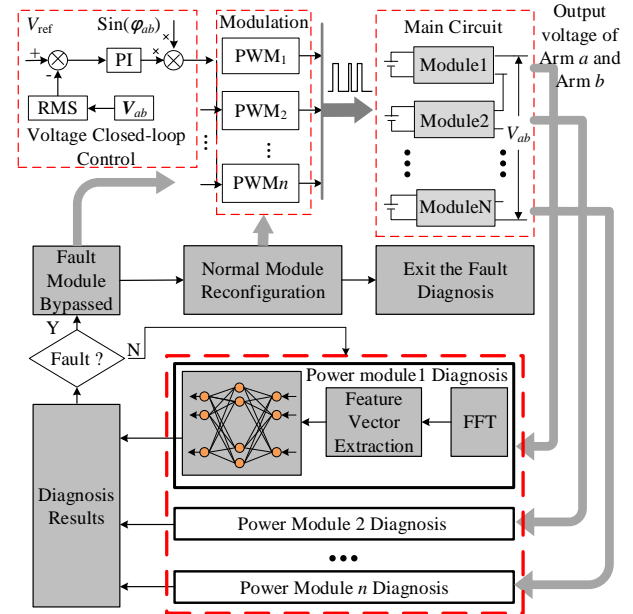
Fig.12 Fault diagnosis and Reconfiguration strategy

The output voltage signals of each module are transformed into feature vectors by FFT. Then the diagnosis result could be obtained. If all 3L-NPC modules are working normally, the next diagnosis period would restart. If OCF is detected, the fault module is bypassed and the modulation parameters are reconfigured according to diagnosis results. The cascaded system will go back to normal utilizing remaining normal modules.

A. Fault module bypass method

All modules of 3L-NPC are redundant to each other. Thus, this structure could work under reconfiguration condition. By disconnecting fault module and compensating through

This article has been accepted for publication in a future issue of this journal, but has not been fully edited. Content may change prior to final publication. Citation information: DOI 10.1109/TIA.2019.2901359, IEEE Transactions on Industry Applications

> REPLACE THIS LINE WITH YOUR PAPER IDENTIFICATION NUMBER (DOUBLE-CLICK HERE TO EDIT) <   8

remaining normal modules, the system could go back to normal status. If all fault switches are located in upper half bridge arm or lower half bridge arm, fault module could be disconnected with internal switches, as shown in TABLE XIII. If the fault switches are located in upper and lower half bridge arm, fault module could be disconnected with external circuit.

TABLE XII
GATE DRIVE SIGNALS OF FAULT MODULE

Fault Location	Bypass drive signals							
	Sa1	Sa2	Sa3	Sa4	Sb1	Sb2	Sb3	Sb4
Sa1/Sa2/Sb1/Sb2	0	0	1	1	0	0	1	1
Sa3/Sa4/Sb3/Sb4	1	1	0	0	1	1	0	0

For example, if the fault switches are located in upper or lower half bridge arm, the bypass drive signals of Arm a and Arm b is 0011 or 1100. The fault current paths when the current is positive or negative are shown in Fig.13 and Fig.14. At this time, a and b have the same voltage and the fault module is bypassed.
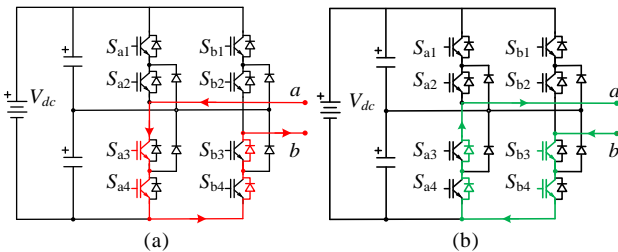

Fig.13 Fault current paths (open circuit faults of upper half bridge arm), (a) when current is positive, (b) when current is negative,
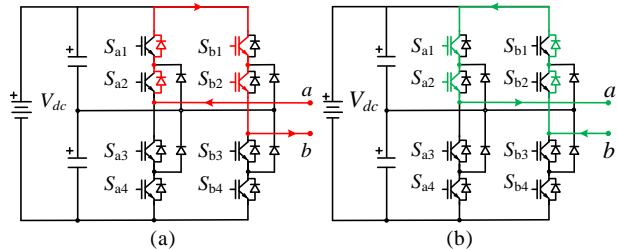

Fig.14 Fault current paths (open circuit faults of lower half bridge arm), (a) when current is positive, (a) when current is negative,

B. Redundant parameter setting

Modulation index M is not only related to voltage effective value, but also related to the number of output voltage level L. THD is decreased as L raises with other conditions unchanged. Basing from theoretical analysis, if $M \in ((j-1)/2N, j/2N)$, L=2j+1, maximum output voltage level L_{max} is 4N+1(j=1,2,… ,2N, N-number of cascaded modules).

In actual application, N-modules cascaded inverter has performance of redundancy. To make $M \in (1-3/2N, 1-2/2N)$ when the inverter is normally working by setting an appropriate DC bus voltage parameter. In this time, L=4N-3. If one fault 3L-NPC module is bypassed, N-1 modules would remain working, and M would be set to $M \in (1-1/(2N-2), 1)$. This process could keep voltage stabilization and keep L constant.

C. Modulation reconfiguration

When a fault module is bypassed, the topology of the cascaded system is changed. If modulation parameters remain unchanged, harmonic performance will not achieve the best possible optimizations. Based on CPS-PWM strategy, carrier phase of each module should be adjusted. Taking an example of the N-modules, modulation reconfiguration strategy is illustrated in Fig.15. When module i is fault and bypassed, the angle of carrier phase shift would change from π/N to π/(N-1).
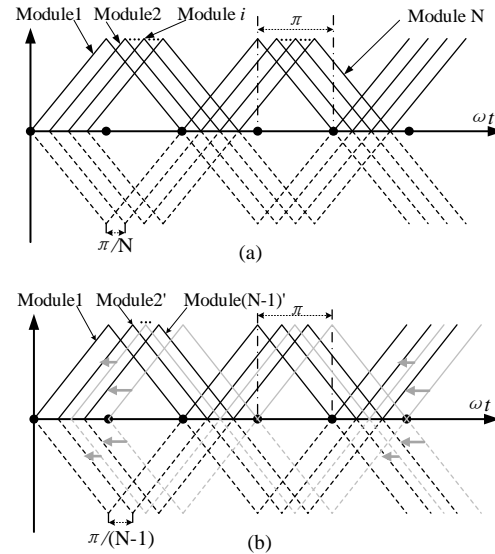

Fig.15 Modulation reconfiguration strategy (a) normal condition. (b) module i is bypassed

VI. SIMULATION AND EXPERIMENT

Simulation verification is implemented in Matlab/Simulink. Table XIII shows the parameters applied in simulation. The simulation model consists of three main power modules, one of them is a redundancy module. RLC loads are used as load of inverter, which is simulated traction power load. RMS value of the output voltage is 27.5 kV and the rated power of system is 9.6MW, which are the same as the train of China high speed railway. A three-layer neural network is designed and the max total of training samples is 800.

TABLE XIII
PARAMETERS OF SIMULATION

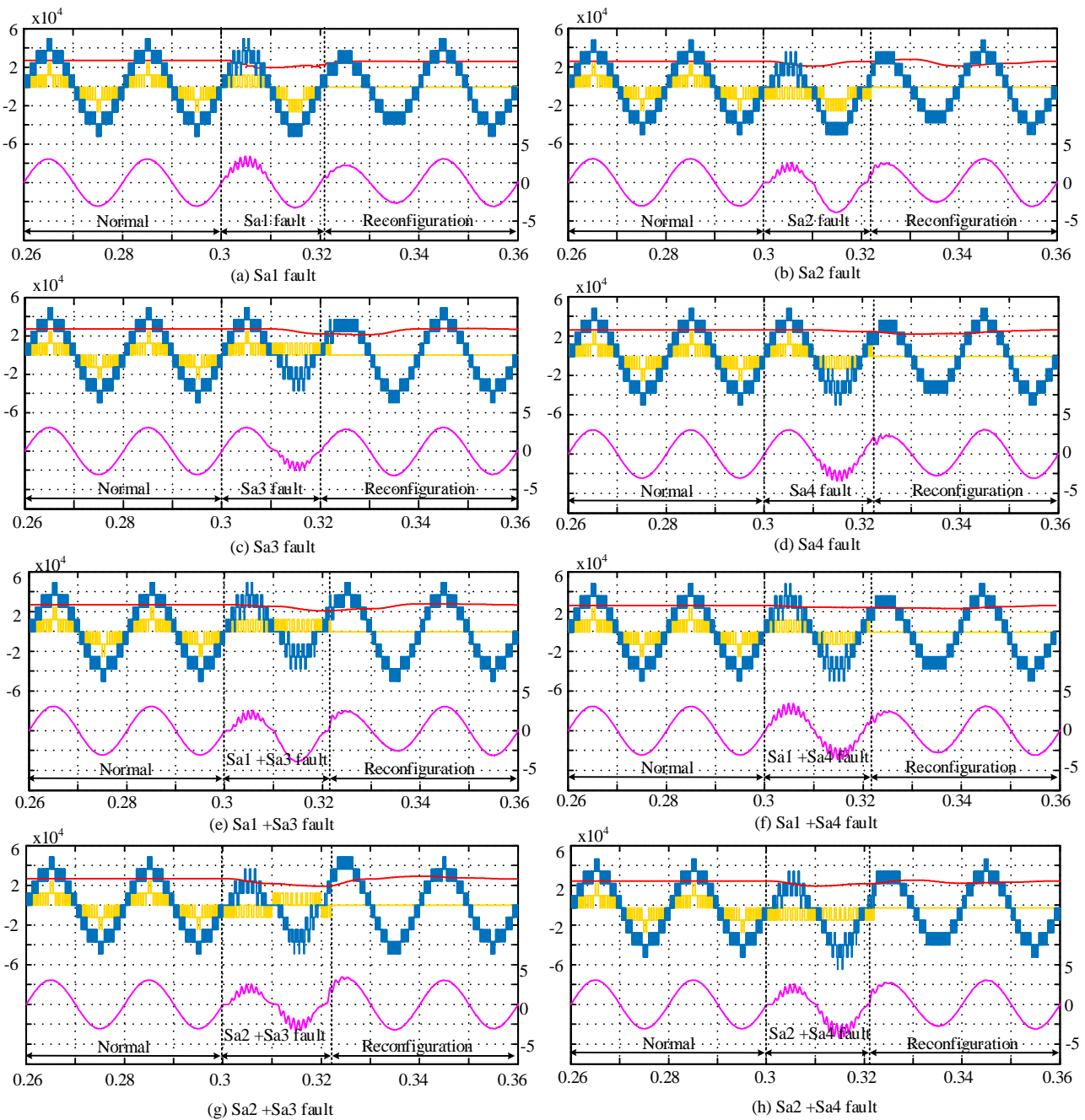| Parameter Name	Parameter Value
Number of modules	3
Redundant module	1
RMS value	27.5kV
DC-link voltage	15kV
Carrier wave frequency	1000 Hz
Power	9.6MW
Load	78Ω
Filter inductor	10mH
Filter capacitor	10μF
Layer of the NN	3
Dimension of hidden layer	8
The max number of training samples	800

Fig.16 Simulation results of 8 fault modes and reconfiguration

Fig. 16(a)-(h) show simulation results of 8 fault modes and reconfiguration strategy. The output voltage of fault module, the output voltage of 3L-NPC-CI, the RMS voltage of 3L-NPC-CI and the current of the load are shown on the picture.

Fig. 16(a) shows simulation results of 3L-NPC-CI reconfiguration in the presence of S_{a1} OCF. The system is operating normally before 0.3s. When the OCF fault occurs at t=0.3s, the output voltage waveform of the fault 3L-NPC module contains a large number of harmonics components. As a result, the output voltage of 3L-NPC-CI is distorted and the level of the output voltage is reduced. The output effective value is lowered and the output current contains higher

harmonics, which will affect the safe operation of the train. At 0.3s, the neural network for fault diagnosis is working. After one modulation wave period, the location of the fault switch is diagnosed. At 0.32s, the fault NPC module is bypassed and the system is reconfiguration. The level of the output voltage is back to normal status. The effective value remains 27.5 kV and the higher harmonics of the output current is removed. The 3L-NPC-CI system achieves stable operation after reconfiguration. In conclusion, Fig.16 (b)-(h) show the test of system reconfiguration in other fault modes, which are the similar analyses to the S_{a1} fault. As a result, it is unnecessary to go into details here.
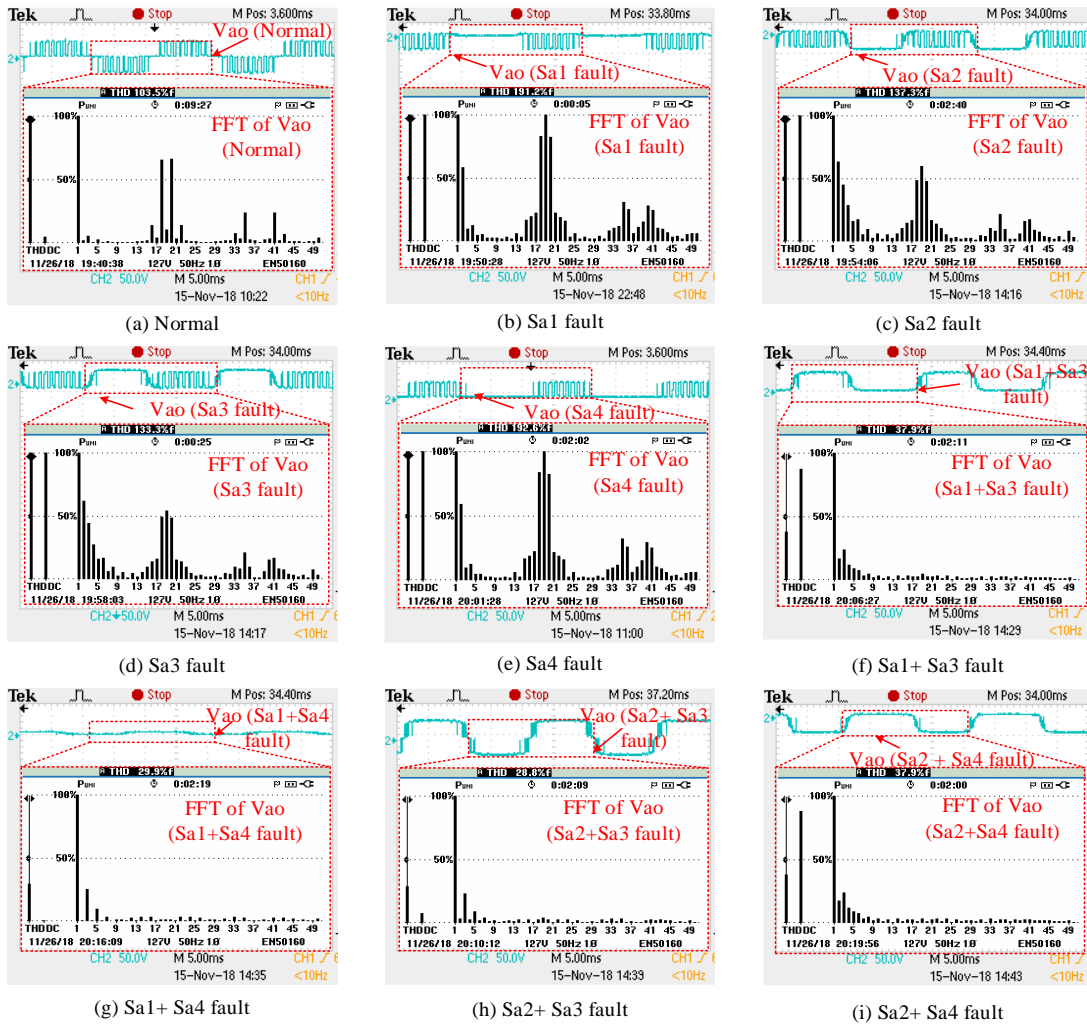
(a) Normal

(b) Sa1 fault

(c) Sa2 fault

(d) Sa3 fault

(e) Sa4 fault

(f) Sa1+ Sa3 fault

(g) Sa1+ Sa4 fault

(h) Sa2+ Sa3 fault

(i) Sa2+ Sa4 fault

Fig.17 Experiment results of 8 fault modes
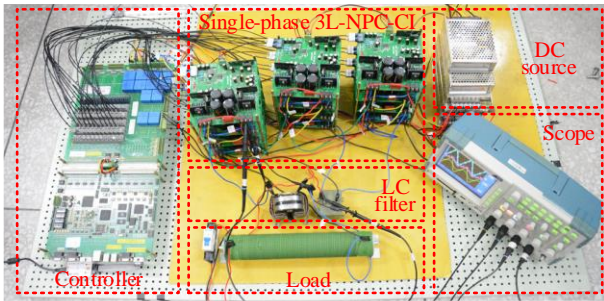
Fig.18 Picture of the Experiment.

TABLE XIV
PARAMETERS OF EXPERIMENT

Parameter Name	Parameter Value
Number of modules	3
Redundant module	1
Controller	EP3C55F484C8
IGBT	IHW20N120R
Voltage sensor	LV-25-P
Current sensor	LA-25-NP
DC-link voltage	50V
Carrier wave frequency	1000 Hz
Load	50Ω
Filter inductor	10mH
Filter capacitor	10μF
Layer of the NN	3
Dimension of hidden layer	8
The max number of training samples	800

In order to verify the correctness of the theoretical analysis, a 3-modules experiment based on the FPGA controller is set up. As shown in Fig.18, the experiment platform consists of 3-modules cascaded inverter, controller, LC filter, load and DC sources. Parameters of the experiment are shown in Table XIV.

Fig. 17 is the experiment result of 8 fault modes. Fig.17 (a) is the normal arm voltage and the harmonics. The voltage of the upper arm and the lower arm is normal. And the normal arm voltage does not have the 2-nd harmonic and the amplitude of DC voltage. The 3-rd harmonic and the 20-th harmonic are lower. The THD of the normal arm voltage is 103.5%. The arm voltage and the harmonics in 8 fault modes are shown in Fig.17 (b)-(i), which are the same as the theoretical analysis in the previous paper. When the single-switch fault occurs, the amplitude of the 3-rd harmonic, the 20-th harmonic and the phase of the 2-nd harmonic are different. When the double-switches fault occurs, the amplitude of the DC voltage, the 2-nd harmonic and the phase of the 2-nd harmonic are different and the 20-th harmonic is almost zero. As these results, the DC amplitude, the fundamental wave amplitude, the 2-nd harmonic amplitude, the 3-rd harmonic amplitude, the 20-th harmonic amplitude and fundamental wave phase angle, the 2-nd harmonic phase angle can be regarded as feature vectors of the fault diagnosis.
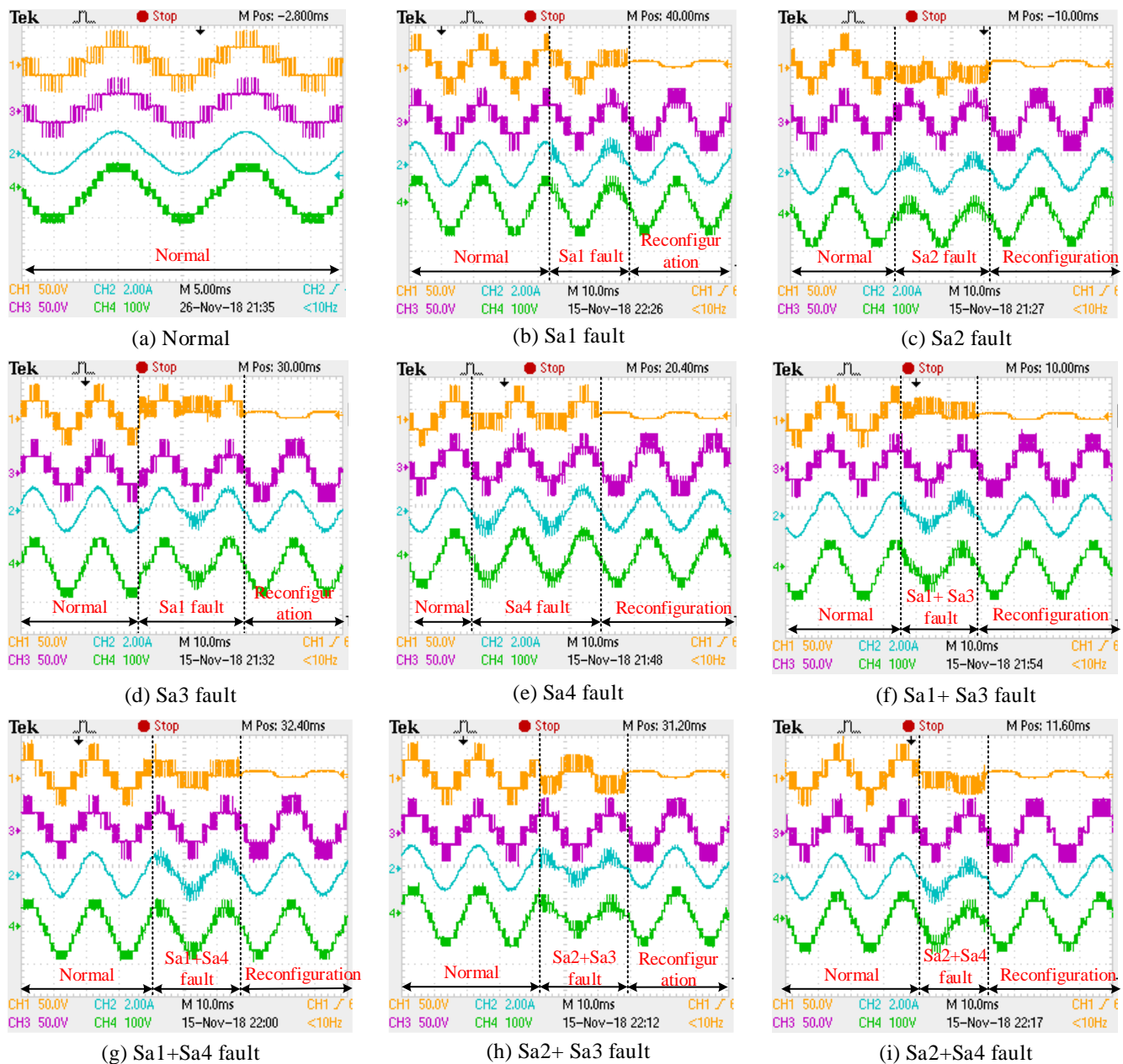
(a) Normal

(b) Sa1 fault

(c) Sa2 fault

(d) Sa3 fault

(e) Sa4 fault

(f) Sa1+ Sa3 fault

(g) Sa1+Sa4 fault

(h) Sa2+ Sa3 fault

(i) Sa2+Sa4 fault

Fig.19 Experiment results of system reconfiguration

The experimental results of the system reconfiguration are shown in Fig.19. CH1 is the output voltage of the fault module. CH2 is the output voltage of normal module. CH3 is the current of the load. CH4 is the output voltage of 3L-NPC-CI. The Fig.19 (a) is the normal status of the 3L-NPC-CI. The output voltage of each NPC module is 5 levels and the output voltage of 3L-NPC-CI is 9 level. The current of the load is sinusoidal with low harmonic.

Fig.19 (b)-(e) are the experimental results of the system reconfiguration when the single-switch OCFs occur in power switch S_{a1}, S_{a2}, S_{a3} and S_{a4}. Fig.19 (f)-(i) is system reconfiguration when the double-switch OCFs occur. When the fault occurs, the output voltage level of the fault NPC module and 3L-NPC-CI is reduced which has higher harmonics. As a result, the current of the load has a lot of higher harmonics.

When the system is in fault operation, the independent output of each module does not affect each other, so that output voltage of non-faulty module is still normal. At this time, the fault diagnosis controller is working. After about a modulation wave period, the fault switches is detected and the reconfiguration strategy is put into operation. As a result, the fault module is bypassed and the output voltage of the fault module becomes 0. Because of the reconfiguration strategy, the modulation index of the non-faulty module is increased. The output voltage level of 3L-NPC-CI is restored 9 levels and the current of the load remains sinusoidal. At this moment, the output voltage of the cascaded system still meets the requirements and the harmonic content is less.

From the simulation and experimental results, the proposed method is able to improve robustness and reliability of 3L-NPC-CI in traction power supply system. The fault diagnosis

and system reconfiguration strategy proposed in this paper is effective and practical.

VII. CONCLUSION

This paper presents a neural network-based fault diagnosis method and reconfiguration strategy for single-phase 3L-NPC-CI. Simulation and experimental results are given to validate the proposed fault diagnosis method and reconfiguration strategy. The proposed method is able to detect open-circuit fault, identify the fault location and reconfigure the output voltage of the single-phase 3L-NPC-CI after the fault module is bypassed. According to the aforementioned analysis and implementation, the following advantages can be obtained. First, the fault switches location can be identified accurately about one modulation period based on the neural network fault diagnosis method. And then, once the faults are identified, reconfiguration strategy can be put into operation to implement fault-tolerant control. After system reconfiguration, the output voltage level and the RMS value of the output voltage remain unchanged. The robustness and reliability of 3L-NPC-CI in traction power supply system is improved by the proposed neural network-based fault diagnosis method and reconfiguration strategy.

REFERENCES

[1] N. Akira, I. Takahashi, and H. Akagi. "A New Neutral-Point-Clamped PWM Inverter." *IEEE Trans. Ind. Appl.,* vol.IA-17, no.5, pp. 518-523, Sept. 1981.

[2] Z. Shu, X. He, Z. Wang, D. Qiu, and Y. Jing, "Voltage Balancing Approaches for Diode-Clamped Multilevel Converters Using Auxiliary Capacitor-Based Circuits," IEEE Transactions on Power Electronics, vol. 28, no. 5, pp. 2111-2124, May. 2013.

[3] Z. Shu, S. Xie, and Q. Li, "Single-Phase Back-To-Back Converter for Active Power Balancing, Reactive Power Compensation, and Harmonic Filtering in Traction Power System," *IEEE Trans. Power Electron.*, vol. 26, no. 2, pp. 334-343, Feb. 2011.

[4] Z. Shu, S. Xie, K. Lu, Y. Zhao, X. Nan, D. Qiu, F. Zhou, S. Gao, and Q. Li, "Digital Detection, Control, and Distribution System for Co-Phase Traction Power Supply Application," *IEEE Trans. Ind. Electron.*, vol. 60, no. 5, pp. 1831-1839, May. 2013.

[5] X. He, Z. Shu, X. Peng, Q. Zhou, Y. Zhou, Q. Zhou, and S. Gao, "Advanced Cophase Traction Power Supply System Based on Three-Phase to Single-Phase Converter," *IEEE Trans. Power Electron.*, vol. 29, no. 10, pp. 5323-5333, Oct. 2014.

[6] X. Peng, X. He, P. Han, H. Lin, S. Gao, and Z. Shu, "Opposite Vector Based Phase Shift Carrier Space Vector Pulse Width Modulation for Extending the Voltage Balance Region in Single-Phase 3LNPC Cascaded Rectifier," *IEEE Trans. Power Electron.*, vol. 32, no. 9, pp. 7381-7393, Sept. 2017.

[7] B. Li, S. Shi, B. Wang, G. Wang, W. Wang, and D. Xu, "Fault Diagnosis and Tolerant Control of Single IGBT Open-Circuit Failure in Modular Multilevel Converters," *IEEE Trans. Power Electron.*, vol. 31, no. 4, pp. 3165-3176, Apr. 2016.

[8] E. L. L. Fabricio, C. B. Jacobina, N. Rocha, R. P. d. Lacerda, and M. B. d. R. Corrêa, "Multilevel Converter Based on Cascaded Three-Leg Converters with Reduced Voltage and Current," *IEEE Trans. Ind. Appl.*, vol. 53, no. 5, pp. 4682-4694, Sept./Oct. 2017.

[9] B. Mirafzal, "Survey of Fault-Tolerance Techniques for Three-Phase Voltage Source Inverters," *IEEE Trans. Ind. Electron.*, vol. 61, no. 10, pp. 5192-5202, Oct. 2014.

[10] H. T. Eickhoff, R. Seebacher, A. Muetze, and E. G. Strangas, "Enhanced and Fast Detection of Open-Switch Faults in Inverters for Electric Drives," *IEEE Trans. Ind. Appl.*, vol. 53, no. 6, pp. 5415-5425, Nov./Dec. 2017.

[11] J. Lamb, and B. Mirafzal, "Open-Circuit IGBT Fault Detection and Location Isolation for Cascaded Multilevel Converters," *IEEE Trans. Ind. Electron.*, vol. 64, no. 6, pp. 4846-4856, Jun. 2017.

[12] X. Ge, J. Pu, B. Gou, and Y. Liu, "An Open-Circuit Fault Diagnosis Approach for Single-Phase Three-Level Neutral-Point-Clamped Converters," *IEEE Trans. Power Electron.*, vol. 33, no. 3, pp. 2559-2570, Mar. 2018.

[13] J. O. Estima, and A. J. M. Cardoso, "A New Algorithm for Real-Time Multiple Open-Circuit Fault Diagnosis in Voltage-Fed PWM Motor Drives by the Reference Current Errors," *IEEE Trans. Ind. Electron.*, vol. 60, no. 8, pp. 3496-3505, Aug. 2013.

[14] S. Jung, J. Park, H. Kim, K. Cho, and M. Youn, "An MRAS-Based Diagnosis of Open-Circuit Fault in PWM Voltage-Source Inverters for PM Synchronous Motor Drive Systems," *IEEE Trans. Power Electron.*, vol. 28, no. 5, pp. 2514-2526, May. 2013.

[15] F. Wu, and J. Zhao, "A Real-Time Multiple Open-Circuit Fault Diagnosis Method in Voltage-Source-Inverter Fed Vector Controlled Drives," *IEEE Trans. Power Electron.*, vol. 31, no. 2, pp. 1425-1437, Feb. 2016.

[16] R. L. de Araujo Ribeiro, C. B. Jacobina, E. R. C. da Silva and A. M. N. Lima, "Fault detection of open-switch damage in voltage-fed PWM motor drive systems," *IEEE Trans. Power Electron*, vol. 18, no. 2, pp. 587-593, March 2003.

[17] T. Kim, W. Lee and D. Hyun, "Detection Method for Open-Circuit Fault in Neutral-Point-Clamped Inverter Systems," *IEEE Trans. Ind. Electron*, vol. 56, no. 7, pp. 2754-2763, July 2009.

[18] W. Chen and A. M. Bazzi, "Logic-Based Methods for Intelligent Fault Diagnosis and Recovery in Power Electronics," *IEEE Trans. Power Electron*, vol. 32, no. 7, pp. 5573-5589, July 2017.

[19] H. Tao, H. Hu, X. Wang, F. Blaabjerg, Z. He, "Impedance-based harmonic instability assessment in multiple electric trains and traction network interaction system, " *IEEE Trans. Ind. Appl.*, vol. 54, no. 5, pp. 5083 - 5096, Sept.-Oct. 2018.

[20] U. Choi, J. Lee, F. Blaabjerg, and K. Lee, "Open-Circuit Fault Diagnosis and Fault-Tolerant Control for a Grid-Connected NPC Inverter," *IEEE Trans. Power Electron.*, vol. 31, no. 10, pp. 7234-7247, Oct. 2016.

[21] T. Kim, W. Lee, and D. Hyun, "Detection Method for Open-Circuit Fault in Neutral-Point-Clamped Inverter Systems," *IEEE Trans. Ind. Electron.*, vol. 56, no. 7, pp. 2754-2763, Jul. 2009.

[22] S. Yang, Y. Tang, and P. Wang, "Seamless Fault-Tolerant Operation of a Modular Multilevel Converter With Switch Open-Circuit Fault Diagnosis in a Distributed Control Architecture," *IEEE Trans. Power Electron.*, vol. 33, no. 8, pp. 7058-7070, Aug. 2018.

[23] V. N. Ghate, and S. V. Dudul, "Cascade Neural-Network-Based Fault Classifier for Three-Phase Induction Motor," *IEEE Trans. Ind. Electron.*, vol. 58, no. 5, pp. 1555-1563, May. 2011.

[24] J. He, R. Katebi, N. Weise, N. A. O. Demerdash, and L. Wei, "A Fault-Tolerant T-Type Multilevel Inverter Topology With Increased Overload Capability and Soft-Switching Characteristics," *IEEE Trans. Ind. Appl.*, vol. 53, no. 3, pp. 2826-2839, May./Jun. 2017.

[25] S. Khomfoi, and L. M. Tolbert, "Fault Diagnosis and Reconfiguration for Multilevel Inverter Drive Using AI-Based Techniques," *IEEE Trans. Ind. Electron.*, vol. 54, no. 6, pp. 2954-2968, Dec. 2007.

[26] S. Mohagheghi, R. G. Harley, T. G. Habetler, and D. Divan, "Condition Monitoring of Power Electronic Circuits Using Artificial Neural Networks," *IEEE Trans. Power Electron.*, vol. 24, no. 10, pp. 2363-2367, Oct. 2009.

[27] J. Li, A. Q. Huang, Z. Liang, and S. Bhattacharya, "Analysis and Design of Active NPC (ANPC) Inverters for Fault-Tolerant Operation of High-Power Electrical Drives," *IEEE Trans. Power Electron.*, vol. 27, no. 2, pp. 519-533, Feb. 2012.

[28] J. Xia, Y. Guo, B. Dai, and X. Zhang, "Sensor Fault Diagnosis and System Reconfiguration Approach for an Electric Traction PWM Rectifier Based on Sliding Mode Observer," *IEEE Trans. Ind. Appl.*, vol. 53, no. 5, pp. 4768-4778, Sep./Oct. 2017.

[29] H. Salimian, and H. Iman-Eini, "Fault-Tolerant Operation of Three-Phase Cascaded H-Bridge Converters Using an Auxiliary Module," *IEEE Trans. Ind. Electron.*, vol. 64, no. 2, pp. 1018-1027, Feb. 2017.

[30] L. F. Costa, G. Buticchi, and M. Liserre, "A Family of Series-Resonant DC–DC Converter With Fault-Tolerance Capability," *IEEE Trans. Ind. Appl.*, vol. 54, no. 1, pp. 335-344, Jun./Feb. 2018.

[31] Y. Wang, X. He, P. Han, X. Peng, Z. Qin, "Fault Diagnosis and System Reconfiguration Strategy of Single-phase Neutral-Point-Clamped Cascaded Inverter," *IEEE ITEC Asia-Pacific*, Ha'erbin, China, 2017.

Pengcheng Han (S'18) was born in Henan, China, in 1992. He received his Bachelor of Science degrees in electrical engineering in 2015 from Southwest Jiaotong University (SWJTU), Chengdu, China, where he is currently working toward obtaining his Doctor of Philosophy degree in electrical engineering. His research interests include multilevel converters, electrified railways, control applications to power electronic converters, and SiC devices and control. His paper Fault Diagnosis and System Reconfiguration Strategy of Single-phase Cascaded Inverter received the Best Paper Award of the IEEE ITEC Asia-Pacific by IEEE Industry Application Society in 2017.

Xiaoqiong He (M'18) received her Bachelor of Science and Doctor of Engineering degrees in electrical engineering from SWJTU, Chengdu, China, in 1998 and 2013, respectively. She joined SWJTU as Teaching Assistant in 1999 and was Lecturer from 2003 to 2008. She is currently Associate Professor in the School of Electrical Engineering in SWJTU. Her research interests include applications to power electronic converters, active power filters, and PWM rectifiers and control.

Haijun Ren was born in Chongqing, China, in 1993. He received the B.S. degree in electrical engineering and information from Southwest Petroleum University, Chengdu, China, in 2017, where he is currently working toward the M.S. degree in Southwest Jiaotong University, majoring in Electrical Engineering. His research interests include electric traction supply system and fault diagnosis.

Yi Wang was born in Neimenggu, China, in 1994. She received her Bachelor of Science degree in electrical engineering in 2016 from SWJTU, Chengdu, China, where she is currently working toward acquiring her Master of Science degree in electrical engineering from the School of Electrical Engineering. Her research interests include inverters connected to the grid, advanced traction power supply system and the technology of fault diagnoses.

Xu Peng (S'18) was born in Sichuan, Chinas in 1987. He received his Bachelor of Science and Master of Science degrees in electrical engineering from SWJTU, Chengdu, China, in 2010 and 2014, respectively. In 2018, he received his Doctor of Engineering degree in electrical engineering from SWJTU, where he is currently working at the Civil Aviation Flight University of China in Guanghan, China. His research interests include electric traction supply systems and power electronic converters.

Zeliang Shu (S'06–M'09–SM'12) received his Bachelor of Science and Doctor of Engineering degrees in electrical engineering from SWJTU, Chengdu, China, in 2002 and 2007, respectively. From 2008 to 2009, he was Lecturer at SWJTU, where he is currently Professor Ph.D. Supervisor in the School of Electrical Engineering. His research interests include multilevel converters, active power filters, reactive power compensators, PWM rectifiers, and digital signal processing and control applications to power electronic converters.

Shibin Gao received the B.S., M.S., and Ph.D. degrees in electrical engineering from Southwest Jiaotong University, Chengdu, China, in 1985, 1988, and 2004, respectively. He is currently a Professor and Ph.D. supervisor in the School of Electrical Engineering, Southwest Jiaotong University. His research interests include the analysis of power supply system, relay protection, and integrated automation in traction power supply system.

Yanbo Wang (S'15-M'17) received Ph.D degree in the department of Energy Technology, Aalborg University, Denmark in 2017. Currently, he is with the department of Energy Technology in Aalborg University as a Postdoctoral Fellow. His research interests include distributed power generation system, wind power system, microgrid, as well as operation and control technologies of power electronic-dominated power system. Dr.Wang's paper on Distributed Power System received the First Prize Paper Award of the 6th International Conference of Smart Grid cosponsored by IEEE Industry Application Society in 2017. He received the Best Session Paper Award at the annual conference of the IEEE Industrial Electronics Society in 2015 in Japan.

Zhe Chen (M'05-SM'08-F'18) received the B.Eng. and M.Sc. degrees from Northeast China Institute of Electric Power Engineering, Jilin City, China, and the Ph.D. degree from University of Durham, U.K. Dr Chen is a full Professor with the Department of Energy Technology, Aalborg University, Denmark. He is the leader of Wind Power System Research program at the Department of Energy Technology, Aalborg University and the Danish Principle Investigator for Wind Energy of Sino-Danish Centre for Education and Research. His research areas are power systems, power electronics and electric machines, and his main current research interests are wind energy and modern power systems. He has led many research projects and has more than 500 publications in his technical field.